Dynamic Electrochemiluminescence Imaging of Single Giant Liposomes Opening at Polarized Electrodes

Fatma Ben Trad, Vincent Wieczny, Jérôme Delacotte, Mathieu Morel, Manon Guille-Collignon, Stéphane Arbault, Frédéric Lemaître, Neso Sojic, Eric Labbé, Olivier O. Buriez, et al.

HAL Id: hal-03552115

https://hal.sorbonne-universite.fr/hal-03552115

Submitted on 2 Feb 2022

Dynamic Electrochemiluminescence Imaging of Single Giant Liposomes Opening at Polarized Electrodes.

Fatma Ben Trad,[a] Vincent Wieczny,[a] Jérôme Delacotte,[a] Mathieu Morel,[a] Manon Guille-Collignon,[a] Stéphane Arbault,[b] Frédéric Lemaître,[a] Neso Sojic,[c] Eric Labbé,[a] and Olivier Buriez[a*].

[a] *PASTEUR, Département de Chimie, Ecole Normale Supérieure, PSL University, Sorbonne Université, CNRS, 75005 Paris, France.*

[b] *Univ. Bordeaux, CNRS, Bordeaux INP, CBMN, UMR 5248 CNRS, F-33600 Pessac, France.*

[c] *University of Bordeaux, CNRS, Bordeaux INP, ISM, UMR CNRS 5255, 33607 Pessac, France.*

ABSTRACT: In this work, the characterization of release events from liposomes has been addressed quantitatively by an electrochemiluminescence (ECL) imaging strategy. First, ECL reagents ($[Ru(bpy)_3]^{2+}$ and tripropylamine) have been encapsulated in sealed giant asymmetrical liposomes (100 µm in diameter) made of DOPG/DOPC phospholipids. After sedimentation on an ITO (Indium Tin Oxide) electrode material, the opening of liposomes was then triggered by polarization of the surface. Under these conditions, amperometry, epifluorescence and ECL were combined and synchronized to monitor and image the rupture of giant liposomes through the release and subsequent ECL emission of their redox content. Amperometry allowed the quantification of the content released from single liposomes. The location and status of liposomes (closed or opened) was assessed by epifluorescence. ECL provided imaging the efflux of matter after liposome opening. This original ECL imaging approach favorably compares to strictly photoluminescent or electrochemical techniques and appears adapted to the investigation of membrane rupture / permeation events.

INTRODUCTION

Liposomes are vesicles composed of a phospholipid bilayer, which attract increasing interest in fields as diverse as targeted drug delivery,[1-3] bioreactors,[4-6] membrane protein science,[7-9] and artificial cells.[10-15] Whatever the liposome size (small: 20 - 50 nm, large: 50 - 100 nm, or giant unilamellar vesicles: 1 - 100 µm),[16, 17] the lipid membrane permeability or opening upon either physicochemical stimulus (temperature, light, pH, redox, etc…) or introduction of e.g. membrane active peptides (cell penetrating peptides, CPPs, or antimicrobial peptides, AMPs)[18, 19] are particularly investigated as model of active and passive lipid barrier crossings.

The electrochemical detection of single liposome collisions upon recording the faradaic current associated to the electron transfer between an electrode and an encapsulated redox species recently proved to allow quantitative representation of the dynamics of the vesicular release.[20] Since electron transfers may not occur across a lipid bilayer, the electroanalytical monitoring of the liposome redox active content after collision and membrane opening at the electrode surface provides accurate information on its rupture/opening mechanisms.[21, 22] Compton and Cheng successfully developed this approach for the real-time quantification of vitamin C content at the single liposome level.[20] Similarly, Ewing and co-workers detected the catecholamine release from single cell liposomes.[23] According to their reports, the so-called *vesicle impact electrochemical cytometry* (VIEC) mostly relates to the electroporation of the liposome on

the polarized electrode, resulting in its rupture and electrolysis of its content.[24-27] Conversely, Bard and co-workers could not detect 100 nm liposomes upon collision with a platinum microelectrode below a threshold concentration of surfactant.[28] More recently, they could show that the permeability of DMPC lipid membranes can also be tuned by the solution temperature when liposomes do not open spontaneously.[29] Actually, both parameters (surfactant concentration and temperature) would be key experimental factors for the liposome membrane electroporation process mentioned by Ewing. Besides, it is well established that the liposome membrane stability is strongly dependent on its lipid composition, on external parameters such as temperature and pH,[30] but also depends on interactions with specific molecules able to weaken, permeabilize, or penetrate the lipid bilayer.[31-38]

Although amperometry is clearly a powerful technique gathering quantitative information on the amount of electroactive species released after the opening of a single liposome with an excellent temporal resolution (~ ms), this approach lacks spatial resolution.[39, 40] Accordingly, single giant liposomes (15-50 µm in diameter) were successfully characterized by scanning electrochemical microscopy (SECM) in which electrochemical signals were measured with micrometric resolution.[41] SECM images of liposomes containing $[Ru(bpy)_3]^{2+}$ (bpy = 2,2'-bipyridine) were obtained and revealed a very low leakage of the ruthenium complex from intact liposomes (made of DSPC/DSPG or DSPC/SOPG in a 80/20 molar ratio). Nevertheless, SECM exhibits a temporal resolution limited by the time required to

1

scan the sample and reconstruct the image of the "electrochemical" activity/ topography of the liposomes, a drawback partially overcome using arrays of soft microelectrodes.[42-44] Alternatively, Bard and Zhan introduced electrochemiluminescence (ECL) labeling, with $[Ru(bpy)_3]^{2+}$-encapsulated in submicrometer-sized liposomes, and its application in a sandwich type immunoassay of human C-reactive protein.[45] However, 100-nanometer size liposomes used in this work were too small for microscopy imaging and a surfactant was required to permeate liposomes and release the ECL label. Recently, Glasscott *et al.* reported a droplet-confined ECL as a quantitative tool to map solvent entrapment in multiphase systems and to visualize the phase boundaries of such systems.[46, 47]

Using liposome-encapsulated luminophores, ECL appears particularly adequate to provide unambiguous signature of extravesicular release events, with a better signal/noise ratio than namely electrofluorochromic probes. Since ECL is an electrochemically triggered process ultimately leading to photon emission,[48, 49] this technique brings important advantages over other optical methods. Firstly, ECL does not require any excitation light source unlike photoluminescence (PL) techniques (i.e., fluorescence or phosphorescence). Therefore, an extremely low photonic background remains, requiring simple instrumentation that can be coupled to microscopy and allowing highly sensitive detection.[50] Secondly, the electrochemical stimulation provides control on the duration of the ECL-emitting region, whereas the optical measurement makes the method extremely sensitive and allows the location of the event to be observed. Thirdly, the current rapid development of electrochemical materials, luminophores[51] and optical devices lead to a significant improvement of the resolution of optical signals. These remarkable characteristics have triggered the development of ECL methods in analytical chemistry and more specifically in bioanalysis.[52-55]

As already mentioned, considering the optical measurement in ECL, a current important development of this technique is its implementation to visualize single objects. On the one hand, single entities such as nanowires,[56] beads for immunoassays,[57-59] collisions of attoliter droplets,[60] graphene oxide nanoparticles,[61] and Janus metallic nanoparticles[62] could be visualized by ECL. On the other hand, effluxes of hydrogen peroxide could be also observed by ECL at the single cell level.[63-66] More recently, ECL was successfully implemented to image membrane proteins,[67] entire plasma membranes of single cells,[68] and ultimately single mitochondria.[69]

From a mechanistic point of view, model chemical systems providing high ECL imaging efficiency feature a ruthenium polypyridine luminophore, $[Ru(bpy)_3]^{2+}$, and tripropylamine (TPrA) as a sacrificial co-reactant. Several competitive mechanistic pathways may simultaneously occur.[70-72] Importantly, the specificity and complexity of these mechanisms resides in the heterogeneous and homogeneous electron-transfer reactions involving the luminophore and the co-reactant for the ECL emission to proceed. Indeed, whatever the mechanism (oxidation of both the co-reactant and the luminophore or oxidation of only the co-reactant), the critical step relies on the occurrence of a homogeneous reaction between both electrogenerated species after a preliminary heterogeneous oxidation step at the electrode surface.

Liposomes obtained from giant unilamellar vesicles are particularly attractive systems thanks to their eligibility to optical microscopy and to various micromanipulation techniques.[73-76] Accordingly, we report here on an original approach to image by ECL the delivery of single giant liposomes content in the extravesicular medium. Furthermore, this ECL imaging was synergistically combined with amperometry and PL to get complementary information on the dynamics and quantification of giant liposome content, as well as on the status of liposomes before and during permeation (location, geometric area, rupture dynamics). ECL generation of single liposomes was monitored after their bursting at the electrode surface. Indeed, a stable liposome lying on a polarized surface and loaded both with the luminophore and the co-reactant should not generate ECL since electron transfer cannot proceed across the membrane of the liposome. However, in case of a membrane opening or rupture, oxidation of the released species should take place at the electrode surface, triggering the emission of light (**Figure 1**).
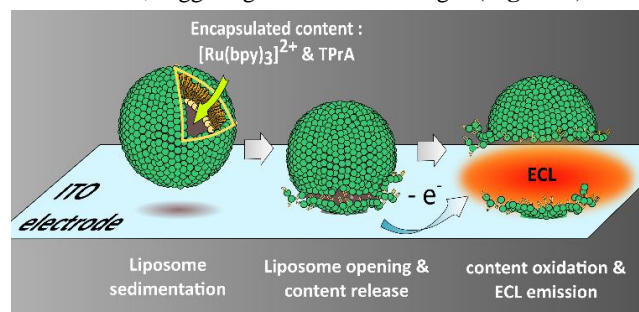

Figure 1. ECL imaging of single giant liposomes opening at polarized electrodes.

More particularly, our original approach relies on collecting both the photonic and amperometric signals produced by ECL generated during and after the rupture of giant liposomes loaded with the luminophore and co-reactant. This strategy required several experimental steps to be achieved. A first step was the successful encapsulation of both $[Ru(bpy)_3]^{2+}$ and TPrA in giant liposomes (~ 50 µm in radius). The choice of the lipids was dictated by their ability to keep liposomes impermeable as long as they are not in contact with the electrode surface. Accordingly, asymmetrical liposomes made of DOPG (on their outer leaflets) and DOPC phospholipids (inner leaflets) had to be prepared. It is noteworthy that these lipids are widely used to explore the translocation of cationic biomolecular species like cell-penetrating peptides.[18, 19]

Secondly, the monitoring of amperometry, PL, and ECL has been carried out in a synchronized way. This led to complementary quantitative and visual information of liposomes coming in contact with the electrode surface followed by their permeation then the release of their content in the extra-vesicular medium. More specifically, there are two inherent values in the use of amperometry: polarization of the indium tin oxide (ITO) surface to induce liposome rupture, and quantification of liposome size. Additionally, amperometry gave access to kinetic and quantitative information on release events from single liposomes. PL provided information on the liposome localization/status whereas ECL allowed monitoring the efflux of luminophores after liposome opening.

2

EXPERIMENTAL SECTION

Lipids. 1,2-Dioleoyl-sn-glycerol-3-phospho-(1'-*rac*-glycerol) sodium salt (DOPG, 10 mg/mL in chloroform), 1,2-dipalmitoyl-sn-glycero-3-phosphoethanolamine-N-(7-nitro-2-1,3-benzoxadiazol-4-yl) ammonium salt (DPPE-NBD, 1 mg/mL in chloroform, λ_{ex} = 460 nm, λ_{em} = 535 nm), and 1,2-dioleolyl-sn-glycero-3-phosphocholine (DOPC, 10 mg/mL in chloroform) were purchased from Avanti Polar Lipids. Molecular structures of the phospholipids used in this work are shown in Supporting Information (see A/ in the Supporting Information (S.I.)).

Chemicals. Tris(2,2′-bipyridyl)dichlororuthenium(II) hexahydrate, mineral oil, tri-*n*-propylamine (TPrA), D-(+)-glucose, sucrose, and Phosphate buffer saline (PBS) tablets (10 mM phosphate, 137 mM sodium chloride; 2.7 mM potassium chloride; pH 7.4) were purchased from Aldrich. All chemicals were used without further modification.

Instrumentations. Electrochemical measurements (cyclic voltammetry) were performed by using an Autolab potentiostat (PGSTAT 20). ECL experiments were performed with a µAUTOLAB Type III and an inverted Zeiss Observer.Z1 microscope placed inside a Faraday cage. An EMCCD camera (C9100-13, Hamamatsu, Japan), connected to the microscope, was used to detect and collect the luminescent signal. PL images were performed with a diode (THORLABS M455L3, λ_{ex} = 455 nm). A Zeiss filter set 74HE was used to illuminate the $[Ru(bpy)_3]^{2+}$ luminophore (λ_{ex} = 450 nm; λ_{em} = 610 nm).

Reactant aqueous solutions. Extra- and intra-vesicular solutions were prepared from highly purified water (resistivity=18 MΩ.cm; Milli-Q system; Millipore, Billerica, MA, USA). The extra-vesicular solution was prepared by dissolving glucose in PBS to reach a final concentration of 0.7 M and an osmolality of around 1000 mOsm.Kg⁻¹. This solution will be referred as the "extra-vesicular solution" in the following. For the intra-vesicular solution, sucrose and TPrA were added in PBS. This led to a 10 mL solution containing sucrose and TPrA at concentrations of 0.7 M and 100 mM, respectively. Under these conditions, a very basic (pH = 10.5) and two-phase mixture was obtained. Nevertheless, addition of concentrated phosphoric acid (around 400 µL at 1 M) allowed to homogenize the solution and to adjust the pH at a value of 7.4 (= Solution S1).

To incorporate the ruthenium complex in the intra-vesicular solution, tris(2,2′-bipyridyl)dichlororuthenium(II) hexahydrate was first added in the above-prepared S1 solution to reach a concentration of 2.5 mM. This solution was then diluted ten times with the S1 solution to reach a final ruthenium concentration of 250 µM. To ensure isotonic conditions, the osmolality had to be sometimes adjusted by adding small amounts of the PBS solution. This final solution (sucrose at 0.7 M in PBS, ruthenium complex at 250 µM, and TPrA at 100 mM) will be referred as the "intra-vesicular solution" in the following.

Phospholipid solutions. Giant liposomes were made of DOPG (outer leaflet) and DOPC (inner leaflet). A small fraction (2 mol%) of DPPE-NBD was also incorporated into each leaflet to allow the liposomes visualization in epifluorescence optical microscopy additionally to their observation by phase contrast. The formation of giant liposomes (see below) required the preliminary preparation of phospholipids in oil suspensions as follows: first, DOPG or DOPC (98 µL; 10 mg/mL in chloroform) and DPPE-NBD (23 µL; 1 mg/mL in chloroform) were mixed

in a 2 mL glass vial. After chloroform evaporation under vacuum (2 hours), mineral oil (2 mL) was then added to dried phospholipids and the corresponding suspension was sonicated (1 hour). In the following these solutions composed of phospholipids dissolved in mineral oil will be referred as the "lipid solution".

Preparation of $[Ru(bpy)_3]^{2+}$ / TPrA encapsulated giant liposomes. The preparation of giant liposomes was performed through two successive steps. The first one consisted in the microfluidic preparation of a water in oil (W/O) emulsion containing the intra-vesicular solution and surrounded by the lipid solution to form the inner leaflet of giant liposomes. The second one consisted in passing the freshly prepared droplets through a water/oil interface containing either the DOPG/DPPE-NBD or DOPC/DPPE-NBD phospholipid mixtures in order to form the outer leaflet (see B/ in S.I.).

First step: Microfluidic drop generators were prepared from PDMS (RTV-615, Momentive) by classical soft-lithography.[77] The channel-embedding part was made by conventional PDMS replica molding of a photolithographed 50 µm thick SU-8 mold (MicroChem, MA). This replica was then pierced for fluidic connections and sealed by a flat PDMS slab using plasma bonding (Diener-femto). The outlet of the microdevice was then cut-open with a sharp blade to form a L x w x h ≅ 10 x 5 x 5 mm³ tip that could fit in a 500 µl microtube. The intra-vesicular solution and lipids-containing oil were co-flowed at a flow-focusing junction of 100 µm wide channels to obtain a monodispersed emulsion of 50 µm radius droplets.

Second step: A DOPG / DPPE-NBD phospholipids monolayer was previously formed in a 500 µL microtube by incubation (4 hours at 45 °C) of a biphasic mixture composed of the extra-vesicular (250 µL) and lipid (200 µL) solutions. The correct drop generation was checked by brightfield microscopy before inserting the tip of the device inside the microtube and freshly prepared droplets were continuously added to the oil phase. After 2-3 hours of droplets addition through the Oil/Water phase most of the liposomes were formed by passive transfer and fall on the bottom of the Eppendorf tube along the density gradient created between sucrose (MW = 342.30 g/mol) and glucose (180.16 g/mol). Finally, the sample was centrifuged (2000 rpm for 15 seconds) in order to recover as many liposomes as possible.

Imaging of GUVs. Giant liposomes were observed on polystyrene surfaces by phase-contrast and fluorescence microscopy (Zeiss Observer.Z1), using N-Achroplan 10x (aperture 0.25) and LD Plan-Neofluar 20x (numerical aperture 0.6) objectives. Fluorescence excitation was provided by a mercury lamp (HXP 120C) and by selecting the right filter to evidence either the NBD-labelled phospholipid (Zeiss filter set 38 HE) or the ruthenium complex (Zeiss filter set 74 HE). During the ECL experiments, PL images were collected as well by illumination with a flashing diode (THORLABS M455L3, λ_{ex} = 455 nm).

Device fabrication for electrochemical and ECL experiments. Optical glass slides (22 mm × 22 mm × 0.13 mm) with 150 nm-thick ITO films (90% In_2O_3/10% SnO_2, ACM, Villiers Saint Frédéric, France) were selected for microelectrodes fabrication in order to afford low electrical resistance (≤ 20 ohms per square) and high transparency.

3

A piece of poly(dimethylsiloxane) (PDMS, RTV-615; Momentive Performance Materials) was cut to the same size as the optical glass side. Then four holes were punched (2 mm in diameter) in the PDMS piece. The ITO modified glass slide and the PDMS piece were then stuck together by treatment with air plasma at 0.46 mbar (Diener-femto) for 1.5 minutes leading thus to four identical wells featuring ITO as working electrodes in the bottom. A 1 mL micropipette tip, playing the role of the electrochemical cell, was then inserted vertically in one hole up to the glass surface, delimiting thus an ITO working electrode with a size being equal to the inner diameter of the micropipette tip (~ 800 µm). To complete the electrochemical cell, an Ag/AgCl wire (1 mm in diameter) and a platinum wire (1 mm in diameter) used as the reference and the counter electrode, respectively, were finally inserted at the top of the micropipette tip (see C/ in S.I.).

Electrochemical experiments. Electrochemical measurements were performed by using an Autolab potentiostat, PGSTAT 20, (cyclic voltammetry) and a µAUTOLAB Type III (chronoamperometry). They were carried out at room temperature in a specific home-made three-electrode cell (see above "Device fabrication"). Accordingly, the reference and counter electrodes were a silver/silver chloride wire and a platinum wire, respectively. The optical glass slide with a 150 nm-thick ITO film played the role of the working electrode.

Combination of ECL / Chronoamperometry / Photoluminescence experiments. Combination of ECL, chronoamperometry and photoluminescence experiments was performed with the same device as that used for pure electrochemical experiments, but with a µAUTOLAB Type III and through an e-corder 401 system (eDAQ Pty Ltd, Australia) associated with the eDAQ Chart software. The ECL signals, coming from the giant liposomes rupture on the ITO surface, were detected by an EMCCD camera (Hamamatsu, Japan) which was connected to an inverted Zeiss LSM 710 microscope inside a Faraday cage. A constant potential value set at +1.2 V vs. Ag/AgCl (used as the reference electrode) was applied to the ITO working electrode. The quality of luminescent images could be optimized by the adjustment of gain, sensitivity as well as the exposure time. Images were registered then treated by using HCImage Live and ImageJ softwares, respectively. To couple ECL and PL during the liposomes permeabilization at the electrode surface it was necessary to use a flashing diode (λ_{ex} = 455 nm) to reveal the ruthenium complex inside liposomes and to correlate the ECL signal with the right liposome (see D/ in S.I.).

Data treatment. The recorded chronoamperograms were analyzed in two steps to extract and deconvolute analyzable amperometric spikes from the raw trace. Firstly, the decay of the baseline current (mostly capacitive origin) was fitted by an exponential law (in two zones before and after the series of amperometric spikes) and subtracted from the raw current. Secondly, isolated spikes were considered for basis of subsequent simulations. Because such peaks showed an exponential decay, we decided to model them with an appropriate mathematical function taking into account both increase and decrease in current. The Weibull function (5 parameters, Sigma 12.0 software) meets such requirements and allows one to describe peaks and gave satisfactory results in our case ($R^2 > 0.99$). This mathematical law was then extended to all overlapped spikes. Therefore, from the full chronoamperogram, the first spike (i.e. starting to

a zero baseline from the first step) was selected. If entirely isolated, no fitting was required. If superimposed with a following event, its non-overlapped portion was fitted by the appropriate Weibull function. The entire spike was thus obtained and subtracted from the whole trace to constitute a new baseline and the other spikes were selected or fitted accordingly. Of note, we finally verified that summing all the extracted spikes led to the initial whole amperometric trace. Finally, the area of the selected/obtained entire amperometric spikes (i.e. the coulometric charge corresponding to the electrochemical detection for each event) were estimated using the trapezoidal approximation.

RESULTS AND DISCUSSION

Encapsulation of ECL reagents in liposomes and visualization of the loaded giant liposomes. To our knowledge, $[Ru(bpy)_3]^{2+}$ has not been encapsulated previously in the presence of TPrA, although introduced as a single species in nanometer and micrometer-size liposomes made of DSPC/DSPG or DSPC/SOPG in 80/20 molar ratios.[41, 45] In a first approach, we decided to prepare symmetrical micrometer-size liposomes made of 1,2-dioleoyl-sn-glycero-3-phosphoglycerol (DOPG), a classical anionic phospholipid used to prepare artificial endosome. However, the choice of the nature of the lipids was also dictated by the fact that the liposomes must remain impermeable as long as they are not in contact with the ITO polarized electrode. The content release must indeed occur only after liposomes came into contact with polarized ITO.

To efficiently fabricate giant liposomes with low polydispersity, we firstly prepared an emulsion from a microfluidic drop generator (see the experimental section and B/ in the S.I.).[78] Accordingly, monodispersed emulsions made of water/sucrose droplets (50 µm in radius) containing the ruthenium complex and surrounded by a monolayer of DOPG phospholipids in an oil phase could be efficiently prepared. Then, the freshly formed droplets were directly passed through an oil-water/glucose column with an interfacial monolayer of DOPG lipids to form the liposome outer leaflet. Under these conditions, giant liposomes with a radius close to 50 µm and containing the ruthenium complex (C = 250 µM) could be obtained.

Unfortunately, the same methodology failed to prepare inner- and outer-DOPG leaflets liposome containing not only $[Ru(bpy)_3]^{2+}$ (250 µM), but also the TPrA co-reactant (100 mM). Besides, the passage of stable DOPG droplets only loaded with the $[Ru(bpy)_3]^{2+}$ complex through an oil-water/glucose column also containing the TPrA (at a concentration of 100 mM) did not produce stable GUVs suggesting that the positively charged form of TPrA destabilized the self-assembling of negatively charged DOPG phospholipids, making unstable droplets and/or liposomes.

Accordingly, the introduction of a zwitterionic phospholipid from the phosphocholine series (DOPC) to form the inner leaflet, while keeping DOPG for the outer leaflet allowed the preparation of asymmetrical GUVs. These liposomes containing both ECL reagents (i.e. $[Ru(bpy)_3]^{2+}$ and TPrA) were found stable on polystyrene surfaces allowing their observation by microscopy (**Figure 2**). As shown in **Figure 2A**, giant liposomes were easily observed by phase contrast microscopy thanks to the difference of refractive index between sucrose and glucose that are present inside and outside of the liposomes, respectively. Moreover, giant liposomes were also visualized by PL

4

microscopy through the excitation of either NBD fluorescent probes localized at the level of the lipid bilayer or the $[Ru(bpy)_3]^{2+}$ luminescent complex present inside liposomes by selecting the right dichroic cubes (**Figure 2B** and **2C**). As expected, PL images of the labelled phospholipids highlighted the homogeneous structure and arrangement of the phospholipids within the liposome membrane. Moreover, the luminescent signal from the ruthenium complex indicates a homogenous distribution of the luminophore inside the liposomes. Microscopy images also showed a low polydispersity in liposome size as expected upon using a microfluidic drop generator. Accordingly, most liposomes had a radius of ca. 50 µm (*vide infra*).

At that point, it was important to check for a possible leakage of the $[Ru(bpy)_3]^{2+}$ complex and/or TPrA in the extra-vesicular medium that could jeopardize our ECL-based strategy. Actually, Bard and co-workers showed by SECM, at a much higher concentration than in the present case (50 mM *vs.* 0.25 mM), the occurrence of a very low leakage of $[Ru(bpy)_3]^{2+}$ from intact micrometer-sized liposomes made of DSPC/DSPG or DSPC/SOPG lipids containing the luminophore.[41] A similar situation could be considered in the presence of both $[Ru(bpy)_3]^{2+}$ complex and TPrA (100 mM) though different lipids were used in the present work. As shown in the following, no ECL signal was detected as long as liposomes were visually intact (absence of deformation and/or membrane rupture). Of note, liposomes were used just after their preparation thus limiting this phenomenon.
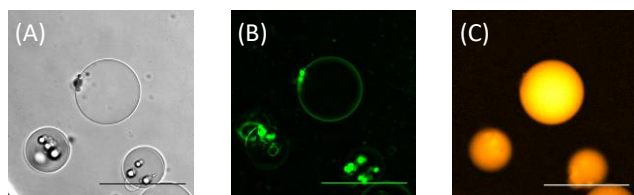

Figure 2. Microscopy images of giant asymmetrical liposomes, made of DOPG / DPPE-NBD (2 mol%) on their outer leaflets and of DOPC / DPPE-NBD (2 mol%) on their inner leaflets, containing $[Ru(bpy)_3]^{2+}$ (C = 250 µM) and TPrA (C = 100 mM). Observation in phase contrast (A) and by PL through the excitation of either (B) NBD fluorescent probes located in membranes or (C) the $[Ru(bpy)_3]^{2+}$ complex located inside liposomes. Note: the small clusters observed in (A) and (B) are oil droplets containing the fluorescent NBD phospholipid. Scale bar: 300 µm.

Electrochemical quantification of liposome content at an ITO polarized surface. The electrochemical detection of a redox compound encapsulated inside liposomes has already been achieved (i) by SECM,[41] (ii) by using a surfactant,[29] (iii) by opening of the liposome membrane when it comes into contact with the electrode surface.[20, 23] Among these various approaches, the latter appears attractive since neither sophisticated apparatus nor extra-stimulus is required. Nevertheless, the opening of liposomes coming into contact with a surface (a strategy commonly used for the preparation of supported bilayer lipid membrane) is not a systematically successful process because the membrane rupture (following adhesion, deformation, and opening steps leading to the spreading of lipids across the surface)[79] depends on various factors including liposome size, temperature, presence of cations, surface charge, surface roughness, ionic strength, solution pH[80] and structural state (i.e. gel or liquid crystalline phases) of lipids within the liposomes.

So far, the release events from liposomes has never been addressed by ECL imaging. In view of this, the stability of our giant liposomes made of DOPG/DOPC/DPPE-NBD was tested on ITO. It is a transparent electrode material commonly used in experiments combining electrochemical and luminescence techniques.[81, 82] Interestingly, liposomes were found to be stable for several minutes on non-polarized ITO, but became unstable when the potential was set at + 1.2 V vs. Ag/AgCl (i.e., a value at which both ECL reagents are oxidized – see E/ and F/ in the S.I.). Note this potential corresponds to the value at which the ECL signal was the most efficient under our experimental conditions (*vide infra*). As already reported, the liposome rupture upon ITO polarization could arise from electroporation of the liposome membrane,[24-27] a key property to achieve electrically-triggered liposome rupture.

To investigate the liposome opening events by amperometry, the giant liposomes were injected in a home-made electrochemical cell (see C/ in the S.I.) with the help of a glass micropipette. They were then let to sediment at the bottom ITO surface of the chamber that was set at a constant anodic potential value of 1.2 V vs. Ag/AgCl. The sedimentation was allowed by the density difference between sucrose inner- and glucose outer-solutions. As shown in **Figure 3**, several current peaks were detected during the sedimentation of liposomes. These current spikes were extracted from the background trace (see G/(A) in S.I. for the raw data), revealing purely faradaic events (**Figure 3A**). In agreement with previous works,[20, 23-29] each spike can be assigned to the oxidation of both the encapsulated $[Ru(bpy)_3^{2+}]$ complex and TPrA that are released when a given liposome collides with the polarized ITO electrode surface. Nevertheless, considering the respective concentration values of the $[Ru(bpy)_3]^{2+}$ complex (250 µM) and of TPrA (100 mM), the current mostly accounts for the oxidation of the amine.

Importantly, the faradaic nature of these peaks was asserted by the fact that no peak was measured at lower oxidation potential values (e.g. +0.50 V), confirming that the current well represents the oxidation of both $[Ru(bpy)_3^{2+}]$ and TPrA species. Another control experiment was conducted at a potential value of +1.2 V in the presence of "empty" liposomes, i.e. not loaded with neither $[Ru(bpy)_3]^{2+}$ nor TPrA. Under these conditions, only a capacitive trace could be observed (see G/(B) in S.I.) confirming that spikes confidently arise from the random collisions of liposomes with the surface of the electrode followed by the release and oxidation of their redox-active content.
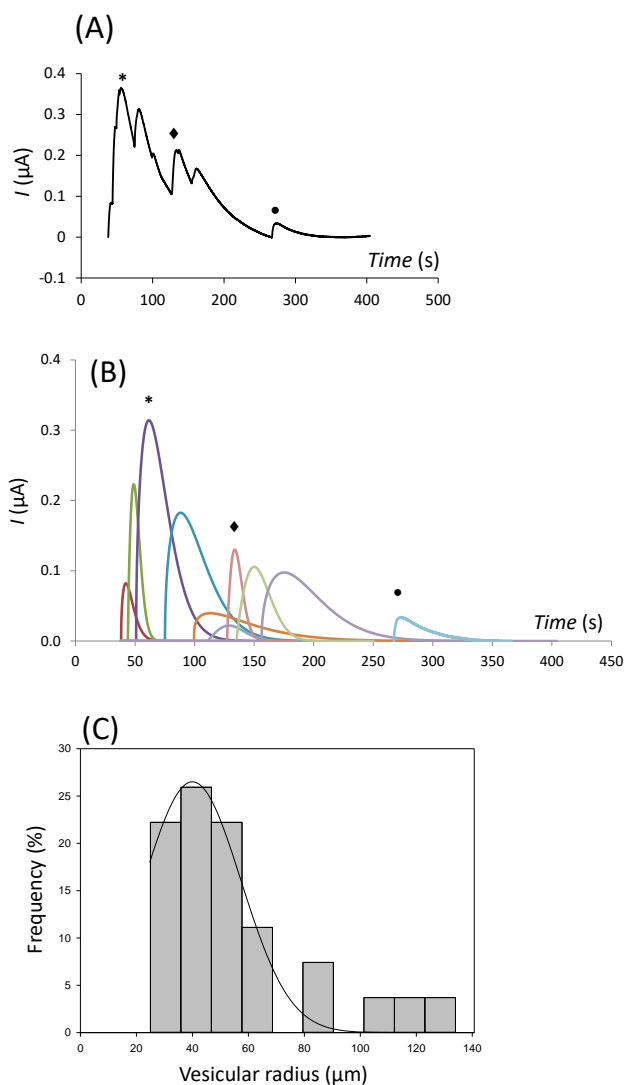
(A)

(B)

(C)

Figure 3. Typical chronoamperograms showing oxidative faradaic traces of TPrA/[Ru(bpy)$_3$]$^{2+}$ encapsulated in single giant liposomes while opening at an ITO electrode surface after (A) subtraction of the capacitive current and (B) deconvolution. Each liposome contained [Ru(bpy)$_3$]$^{2+}$ (C = 250 µM) and TPrA (C = 100 mM). The marked peaks (*,♦,•) allows comparisons before and after deconvolution. The imposed potential was 1.2 V vs. Ag/AgCl. In (C) is exhibited the size distribution of the liposomes (from 27 amperometric events) showing their Frequency (%) as a function of their radius (binning = 10 µm). A modeling from a Gaussian function is also shown (solid line).

Interestingly, the shapes of amperometric peaks resemble those obtained for vesicular releases involved in biological processes (e.g. exocytosis or oxidative stress) although with different time scales.[83] Accordingly, a similar mathematical treatment was carried out to extract the strictly faradaic contribution of these responses. Furthermore, considering that several liposome opening events may overlap, superimposed peaks were deconvoluted introducing adapted mathematical treatment (see the Experimental part).[84] In few words, incremented subtraction of each simulated spike allows the extraction of each event as an

isolated and analyzable amperometric spike (compare **Figures 3A** and **3B)** before and after deconvolution. These spikes are thus related to entire redox released contents. Of note, the sum of all reconstructed peaks obviously leads to the initially measured whole trace. It consequently affords the calculation of the coulometric charge passed during oxidation of the released content from individual liposomes, i.e. by integrating each individual peak. Considering that TPrA was loaded at a concentration of 100 mM inside each liposome, the apparent liposome radius (*R*) was determined for each spike (**Figure 3C**). A mean radius of 55 ± 5 µm was eventually obtained by using Equation (1):

$$Q = nF \times CV = \frac{4}{3}\pi nFCR^3$$

(1)

where *Q* is the measured charge, *F* is the Faraday constant, *C* is the concentration of TPrA in the liposome, and *n* is the number of electrons transferred per molecule during oxidation (*n* = 1 for TPrA in a first order approximation)[20, 83]. The frequency of the events (spikes) was plotted against the apparent radius distribution of the liposomes, taking a binning of 10 µm as a function of their radius. As expected, most of the liposomes exhibit a reconstructed apparent radius close to the one of the original droplets (~ 50 µm) thus reflecting a complete oxidation of the liposome content. Apparent radii below 50 µm could therefore account for partial oxidation or release. Conversely, values larger than 50 µm may represent the fusion of several droplets after their microfluidic preparation. Finally, the rising time of a given amperometric spike is in the range of a few seconds that is rather slow compared to colliding particles. From a kinetic point of view, this suggests that a given event monitored by amperometry is the convolution of two distinct regimes as already observed in similar biological objects[83, 85]: 1) opening of the liposome at relatively short times 2) diffusion of the liposome redox content within the solution at longer times. The observed rising time in our case may therefore result from the liposome deformation due to its starting opening. Such a "convective" regime is further confirmed by ECL analyses (see below).

ECL imaging of giant liposomes opening. As demonstrated above, electrochemical investigations clearly confirmed that amperometry is a powerful technique gathering quantitative information on the amount of electroactive species released after the opening of a single liposome. The next step was to implement the combination of amperometry with both ECL and epifluorescence imaging to visualize the spatial opening/rupture of liposomes and the corresponding release of their content in the extra-vesicular medium, respectively.

Since both luminescent signals (ECL and PL) were registered with the same EMCCD camera all along the experiments, the diode (λ$_{ex}$ = 455 nm) was set in a flashing mode to better distinguish between ECL and PL signals. The images were registered continuously with a 4 frame per second acquisition rate corresponding to 4 Hz frequency. For each second, the first frame (i.e., #1, #5, #9, etc…) was kept as a PL image whereas the third one (i.e., #3, #7, etc…) was selected as an ECL image (**Figure 4**). The two other frames (e.g. #2 and #4 in the first second) were not selected to avoid any PL pollution on ECL images (The PL signal intensity was much higher than the ECL one; see Figure 6).

6

This also explains the acquisition time difference of 500 ms between PL and ECL images. Note that the amperometric signal (noted as "Electrochemistry" in Figure 4) was registered all along each experiment. Accordingly, ECL and PL images could be recorded separately then reassembled to build two series of ECL and PL images as a function of time (in S.I. are shown two videos built from two typical series of both ECL and fluorescence images).
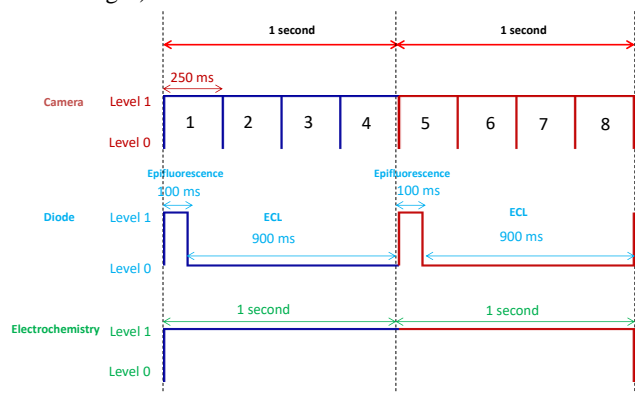

Figure 4. Appropriate time-sequences for the combined detection of amperometry-ECL-PL signals.

As for chronoamperometric experiments, the liposomes containing both the luminophore and TPrA were dropped into the cell and let to sediment at the bottom ITO surface of the chamber (still hold at a potential value of 1.2 V/Ag/AgCl). As a result, the corresponding oxidation of both ECL reagents led to the most efficient ECL signal (see F/ in S.I.). Furthermore, at this potential value the oxidation mechanism is very likely the one featuring the oxidation of both the luminophore and the amine.[68-70]

Figure 5 displays two typical series of ECL and PL images recorded before and during the opening of a given liposome. Interestingly, PL and ECL images brought complementary information. In the sequence of PL images shown in **Figure 5**, the opening and rupture of a liposome could be easily identified (see the liposome location circled in red based on its maximum diameter).

First, the liposome underwent deformation (between 2 and 3 seconds), then rupture (after 3 seconds). Importantly, no ECL signal was detected as long as the liposome was visually intact (before its deformation) confirming the absence of detectable leakage of liposome content in the vicinity of the electrode. However, an ECL signal appeared as soon as the liposome deformed, constituting an optical signature of the release and detection of its content. The ECL process became more efficient as the liposome collapsed. Moreover, the ECL images also show the time and space dispersion of the liposome content outside the liposome. The dark spot observed in ECL corresponds to the contact point between the liposome and the ITO surface. In this area, no light can be electrogenerated since the locally-deposited phospholipid bilayer barrier blocks the ITO electrode surface and the oxidation of the ECL reagents.
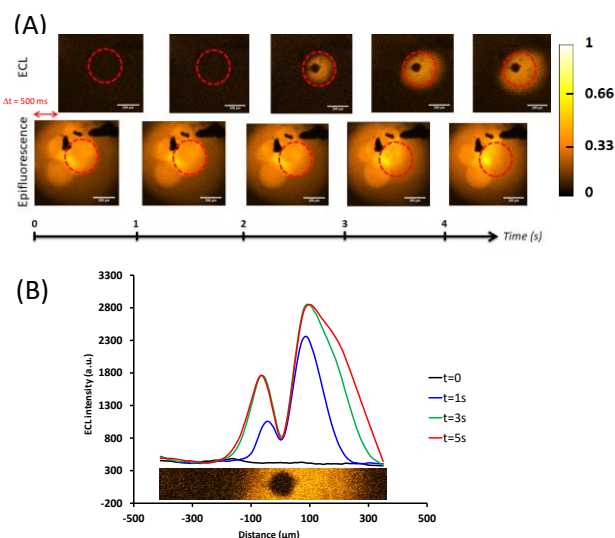

Figure 5. (A) Combination of ECL (top) and PL (below) imaging showing the permeation of a liposome (the one circled in red) made of DOPG/DOPC phospholipids and containing both $[Ru(bpy)_3]^{2+}$ (250 µM) and TPrA (100 mM), as a function of time. To avoid any overlap between both types of visual information, the ECL and PL images have an initial image acquisition time difference of 500 ms. The focus was made at the ITO electrode surface while ECL and PL imaging. Red circles in PL and ECL represent the typical region of interest (ROI) taken in account for the quantitative analyses of the corresponding intensities. (B) Profile of the ECL intensity obtained from (A). Note: dark spots observed in epifluorescence are due to impurities stuck at the electrode surface. Scale bar: 200 µm.

The opening/rupture of liposomes could also be quantified from PL and ECL intensities within specific ROIs as the one delimited in **Figure 5**. As clearly shown in **Figure 6**, combining the three signals provided a comprehensive monitoring of a single liposome opening/rupture and content release. The PL signal appeared first and increased as a liposome approached the transparent ITO surface (the microscopic focus was set at the electrode surface in these experiments). After reaching a maximum intensity, the PL signal rapidly decreased while the faradaic current increased in agreement with the liposomal membrane opening. The fast oxidation of both $[Ru(bpy)_3]^{2+}$ and TPrA generated an ECL signal whose maximum value overlapped the maximum current of the amperometric spike. The ECL signal duration was rather long (around 20 seconds) and decreased faster than the oxidation current. At this stage it is important to note that contrary to the current signal that mostly accounts for the oxidation of the amine, the PL and ECL signals depend on the luminophore concentration. As shown below, the brutal liposome opening led to a very fast dilution of the ruthenium complex involving a convective step. Then a diffusion regime takes place during a longer time scale. These different time scales between the convective and diffusion steps explain the faster decay of the PL signal compared to the ECL one (Figure 6(A)).
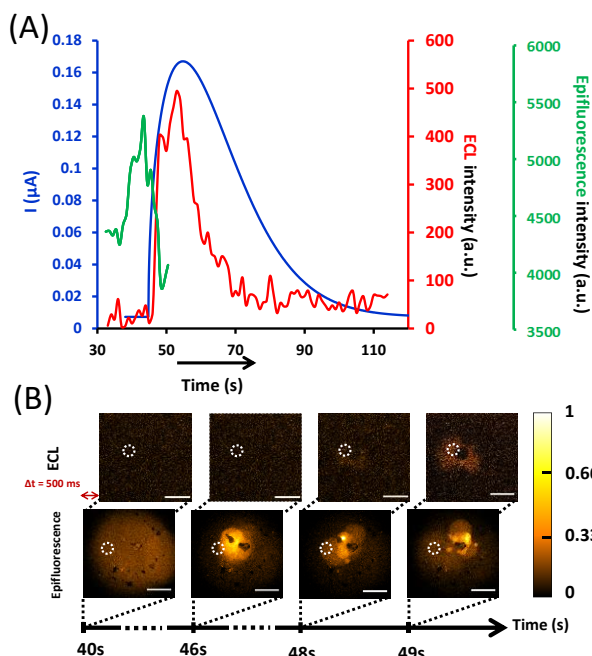
Figure 6. (A) Typical combination of amperometry (blue curve), PL (green curve) and ECL (red curve) quantitative information obtained as a function of time for a single liposome opening at a polarized ITO surface (shown in (B)). Note: above 50 seconds, the epifluorescence (PL) signal was "polluted" by other luminescent liposomes sedimenting in the vicinity of the investigated one. The PL signal in (A) was therefore cut at 50 s. Scale bar: 200 µm.

Interestingly and as shown in **Figures 5 or 6**, ECL imaging allows the dispersion of the luminophore $[Ru(bpy)_3]^{2+}$ to be monitored overtime. The evolution of the apparent distance (δ) of propagation of the light spot was recorded overtime for ten liposomes. A convective spreading was observed at short times due to both the density gradient between inner and outer solutions once the liposome opens and the perturbation caused by the liposome bursting. For seven of the investigated liposomes the spreading of the light spot exhibited the onset of a diffusion regime at times ranging from 0.5 s to 4.5 s depending on the amount of released content. **Figure 7** represents the typical square spreading distance of the apparent light front (δ^2) with time and features the convective regime (for t < 4.5 s) and the diffusion regime (for t > 4.5 s). The boundary between the convective and the diffusion steps was evaluated comparing the spreading velocity of the ECL light spot ($v=\Delta\delta/\Delta t$) with the characteristic diffusion velocity ($v_D=D/\Delta\delta$), considering a generic value of D = 5×10^{-6} cm²/s for the diffusion coefficient of small analytes like $[Ru(bpy)_3]^{2+}$ in moderately viscous aqueous solution (see H/ in the S.I.). Under our conditions, we considered that the diffusion regime can be then characterized by (v/v_D) values lower than 10^{-1}. The diffusion driven part of the spreading curves (δ^2 vs. t) were fitted with a linear function. The fitted value of the slope $20\times10^{-6} \pm 3.10^{-6}$ cm²/s (mean ± standard error of the mean, n = 7 liposomes) was consistent with the expected value $4D = 20.10^{-6}$ cm²/s in a two-dimension spreading at the electrode.
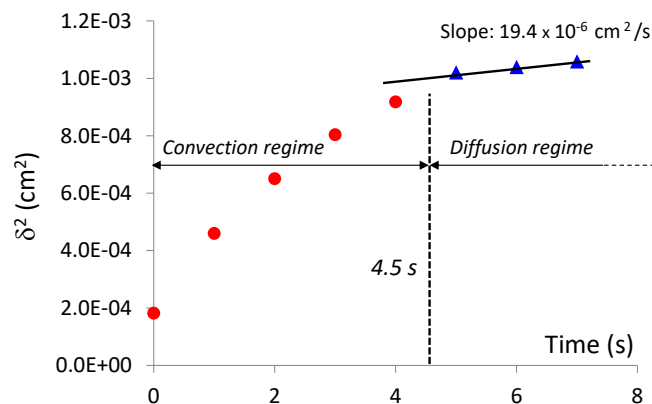

Figure 7. Typical plot showing the evolution of the square of the apparent distance (δ^2) of propagation of the ECL light spots as a function of time. The diffusion coefficient D (4.9×10^{-6} cm²/s) was estimated from the slope (4D) of the linear fitting function (blue triangles). For $n_{liposome}$ = 7, the fitted value of the slope was $20\times10^{-6} \pm 3.10^{-6}$ cm²/s.

CONCLUSION

The opening of giant liposomes loaded with ECL reagents ($[Ru(bpy)_3]^{2+}$ and TPrA) was characterized by the synchronized recording of the faradaic current (amperometry) and the collection of PL and ECL images. Each of these techniques provided complementary information: (i) amperometry enabled a real time and quantitative measurement of the release dynamics of the content from single liposomes; (ii) PL provided information on the status of the liposomes before and during permeation (location, diameter, rupture); (iii) ECL imaging allowed visualization of the release of the liposome content in the extra-vesicular medium after opening. The combination of these three techniques constitute a powerful approach to the accurate characterization of single liposome permeation or opening events with a good spatial and temporal resolution, as well as a quantification of the liposome content. Though TPrA has been used previously on living cells and mitochondria, its relative toxicity may constitute a potential issue for future biological experiments on living matter. However, TPrA may be replaced easily by less toxic co-reactants such as diethanolamine or 2-(dibutylamino)ethanol. This undoubtedly opens avenues in the fields of drug delivery, bioreactors, or artificial cells for which permeation, opening, or trafficking are central issues.

ASSOCIATED CONTENT

Supporting Information

The Supporting Information is available free of charge on the ACS Publications website.

Molecular structure of the phospholipids; Preparation of $[Ru(bpy)_3]^{2+}$ / TPrA encapsulated giant liposomes; Experimental device allowing combination of amperometry and luminescence techniques; Cyclic voltammetry experiments of ECL reagents; Determination of the best oxidation potential value for the most efficient ECL signal; Deconvolution of the pure faradaic current from a whole chronoamperogramm containing a capacitive decay; Determination of the diffusion coefficient of $[Ru(bpy)_3]^{2+}$ (PDF). ECL and photoluminescence videos (MP4).

AUTHOR INFORMATION

Authors

Neso Sojic. orcid.org/0000-0001-5144-1015

Corresponding Author

Olivier Buriez - *PASTEUR, Département de Chimie, Ecole Normale Supérieure, PSL University, Sorbonne Université, CNRS, 75005 Paris, France. Orcid.org/0000-0001-5452-1942 ; Phone : +33 1 44 32 32 62 ;*
Email : olivier.buriez@ens.psl.eu

Notes
There are no conflicts to declare.

REFERENCES

(1) Torchilin, V.P. Recent advances with liposomes as pharmaceutical carriers. *Nat. Rev. Drug Discov.* **2005**, *4*, 145−160.

(2) Allen, T. M.; Cullis, P. R. Liposomal drug delivery systems: From concept to clinical applications. *Adv. Drug Deliv. Rev.* **2013**, *65*, 36–48.

(3) Pattni, B. S.; Chupin, V. V.; Torchilin, V. P. New Developments in Liposomal Drug Delivery. *Chem. Rev.* **2015**, *115*, 10938−10966.

(4) Noireaux, V.; Libchaber, A. A vesicle bioreactor as a step toward an artificial cell assembly. *Proc. Natl. Acad. Sci. U. S. A.* **2004**, *101*, 17669−17674.

(5) Mansy, S. S.; Schrum, J. P.; Krishnamurthy, M.; Tobe, S.; Treco, D. A.; Szostak, J. W. Template-directed synthesis of a genetic polymer in a model protocell *Nature* **2008**, *454*, 122−125.

(6) Bolinger, P. -Y.; Stamou, D.; Vogel, H. Integrated nanoreactor systems: Triggering the release and mixing of compounds inside single vesicles. *J. Am. Chem. Soc.* **2004**, *126*, 8594−8595.

(7) Zimmerberg, J.; Kozlov, M. M. How proteins produce cellular membrane curvature. *Nat. Rev. Mol. Cell Biol.* **2006**, *7*, 9−19.

(8) Bangham, A. D.; Hill, M. W.; Miller, N. G. A. In *Methods in Membrane Biology*; Korn, E. D., Ed.; Springer US: Boston, MA, **1974**; Vol. 1, pp 1−68.

(9) Früh, V.; IJzerman, A. P.; Siegal, G. How to Catch a Membrane Protein in Action: A Review of Functional Membrane Protein Immobilization Strategies and Their Applications. *Chem. Rev.* **2011**, *111*, 640− 656.

(10) Adamala, K.; Szostak, J. W. Nonenzymatic Template-Directed RNA Synthesis Inside Model Protocells. *Science* **2013**, *342*, 1098−1100.

(11) Saito, H.; Kato, Y.; Le Berre, M.; Yamada, A.; Inoue, T.; Yosikawa, K.; Baigl, D. Time-Resolved Tracking of a Minimum Gene Expression System Reconstituted in Giant Liposomes. *ChemBioChem.* **2009**, *10*, 1640−1643.

(12) Szostak, J. W.; Bartel, D. P.; Luisi, P. L. Synthesizing life. *Nature* **2001**, *409*, 387−390.

(13) Kurihara, K.; Okura, Y.; Matsuo, M.; Toyota, T.; Suzuki, K.; Sugawara, T. A recursive vesicle-based model protocell with a primitive model cell cycle. *Nat. Commun.* **2015**, *6*, 8352.

(14) Osawa, M.; Erickson, H. P. Liposome division by a simple bacterial division machinery. *Proc. Natl. Acad. Sci. U. S. A.* **2013**, *110*, 11000−11004.

(15) Deshpande, S.; Caspi, Y.; Meijering, A. E. C.; Dekker, C. Octanol-assisted liposome assembly on chip. *Nat. Commun.* **2016**, *7*, 10447.

(16) Walde, P.; Cosentino, K.; Engel, H.; Stano, P. Giant Vesicles: Preparations and Applications. *ChemBioChem.* **2010**, *11*, 848-865.

(17) Luisi, P. L.; Walde, P. *Giant Vesicles*, John Wiley & Sons Ltd.: New York, **2000**.

(18) Guidotti, G.; Brambilla, L.; Rossi, D. Cell-Penetrating Peptides: From Basic Research to Clinics. *Trends Pharmacol. Sci.* **2017**, *38*, 406–424.

(19) Bechara, C.; Sagan, S. Cell-penetrating peptides: 20 years later, where do we stand?. *FEBS Lett.* **2013**, *587*, 1693-1702.

(20) Cheng, W.; Compton, R. G. Investigation of Single-Drug-Encapsulating Liposomes using the Nano-Impact Method. *Angew. Chem. Int. Ed.* **2014**, *53*, 13928 –13930.

(21) Cannes, C.; Kanoufi, F.; Bard, A.J. Cyclic voltammetry and scanning electrochemical microscopy of ferrocenemethanol at monolayer and bilayer-modified gold electrodes. *J. Electroanal. Chem.* **2003**, *547*, 83-91.

(22) Labbé, E.; Buriez, O. Electrode-supported and free-standing bilayer lipid membranes: Formation and uses in molecular electrochemistry. *Electrochem. Sci. Adv.* **2021**; e2100170. https://doi.org/10.1002/elsa.202100170.

(23) Dunevall, J.; Fathali, H.; Najafinobar, N.; Lovric, J.; Wigström, J.; Cans, A.-S.; Ewing, A. G. Characterizing the Catecholamine Content of Single Mammalian Vesicles by Collision-Adsorption Events at an Electrode. *J. Am. Chem. Soc.* **2015**, *137*, 4344−4346

(24) Lovrić, J.; Najafinobar, N.; Dunevall, J.; Majdi, S.; Svir, I.; Oleinick, A.; Amatore, C.; Ewing, A. G. On the mechanism of electrochemical vesicle cytometry: chromaffin cell vesicles and liposomes. *Faraday Discuss.* **2016**, *193*, 65−79.

(25) Li, X.; Dunevall, J.; Ren, L.; Ewing, A. G. Mechanistic Aspects of Vesicle Opening during Analysis with Vesicle Impact Electrochemical Cytometry. *Anal. Chem.*, **2017**, *89*, 9416−9423.

(26) Li, X.; Ren, L.; Dunevall, J.; Ye, D.; White, H. S.; Edwards, M. A.; Ewing, A. G. Nanopore Opening at Flat and Nanotip Conical Electrodes during Vesicle Impact Electrochemical Cytometry. *ACS Nano* **2018**, *12*, 3010−3019.

(27) Najafinobar, N.; Lovrić, J.; Majdi, S.; Dunevall, J.; Cans, A.-S.; Ewing, A. G. Excited Fluorophores Enhance the Opening of Vesicles at Electrode Surfaces in Vesicle Electrochemical Cytometry. *Angew. Chem., Int. Ed.*, **2016**, *55*, 15081−15085.

(28) Lebègue, E.; Anderson, C. M.; Dick, J. E.; Webb, L. J.; Bard, A. J. Electrochemical Detection of Single Phospholipid Vesicle Collisions at a Pt Ultramicroelectrode. *Langmuir,* **2015**, *31*, 11734−11739.

(29) Lebègue, E.; Barrière, F.; Bard, A. J. Lipid Membrane Permeability of Synthetic Redox DMPC Liposomes Investigated

by Single Electrochemical Collisions. *Anal. Chem.* **2020**, *92*, 2401−2408.

(30) Sułkowski, W. W.; Pentak, D.; Nowak, K.; Sułkowska, A. The influence of temperature, cholesterol content and pH on liposome stability. *J. Mol. Struct.* **2005**, *744*, 737−747.

(31) Xu, D.; Cheng, Q. J. Surface-bound lipid vesicles encapsulating redox species for amperometric biosensing of pore-forming bacterial toxins. *J. Am. Chem. Soc.* **2002**, *124*, 14314−14315.

(32) Ciobanasu, C.; Dragomir, I.; Apetrei, A. The penetrating properties of the tumor homing peptide LyP-1 in model lipid membranes. *J. Pept. Sci.* **2019**, *25*, e3145.

(33) Mahendra, A.; James, H. P.; Jadhav, S. PEG-grafted phospholipids in vesicles: Effect of PEG chain length and concentration on mechanical properties. *Chem. Phys. Lipids* **2019**, *218*, 47−56.

(34) Zylberberg, C.; Matosevic, S. Pharmaceutical liposomal drug delivery: a review of new delivery systems and a look at the regulatory landscape. *Drug Deliv.* **2016**, *23*, 3319−3329.

(35) Brander, S.; Jank, T.; Hugel, T. AFM Imaging Suggests Receptor-Free Penetration of Lipid Bilayers by Toxins. *Langmuir* **2019**, *35*, 365−371.

(36) Nasir, M. Z. M.; Jackman, J. A.; Cho, N. -J.; Ambrosi, A.; Pumera, M. Detection of Amphipathic Viral Peptide on Screen-Printed Electrodes by Liposome Rupture Impact Voltammetry. *Anal. Chem.* **2017**, *89*, 11753−11757.

(37) Jackman, J. A.; Saravanan, R.; Zhang, Y.; Tabaei, S. R.; Cho, N. -J. Correlation between Membrane Partitioning and Functional Activity in a Single Lipid Vesicle Assay Establishes Design Guidelines for Antiviral Peptides. *Small* **2015**, *11*, 2372−2379.

(38) Rose, L.; Jenkins, A. T. A. The effect of the ionophore valinomycin on biomimetic solid supported lipid DPPTE/EPC membranes. Bioelectrochemistry **2007**, *70*, 387−393.

(39) Barlow, S.T.; Figueroa, B.; Fu, D.; Zhang, B. Membrane Tension Modifies Redox Loading and Release in Single Liposome Electroanalysis. *Anal. Chem.* **2021**, *93*, 3876−3882.

(40) Choi, Y.; Park, C.; Kang, Y.; Muya, J. T.; Jang, D. P.; Chang, J. Temporally Resolved Electrochemical Interrogation for Stochastic Collision Dynamics of Electrogenerated Single Polybromide Droplets. *Anal. Chem.* **2021**, *93*, 8336−8344.

(41) Zhan, W.; Bard, A. J. Scanning electrochemical microscopy. 56. Probing outside and inside single giant liposomes containing Ru(bpy)$_3^{2+}$. *Anal. Chem.* **2006**, *78*, 726–733.

(42) Lin, T. -E.; Rapino, S.; Girault, H. H. Lesch, A. Electrochemical imaging of cells and tissues. *Chem. Sci.* **2018**, *9*, 4546-4554.

(43) Lesch, A.; Vaske, B.; Meiners, F.; Momotenko, D.; Cortés-Salazar, F.; Girault, H. H.; Wittstock, G. Parallel Imaging and Template-Free Patterning of Self-Assembled Monolayers with Soft Linear Microelectrode Arrays. *Angew. Chem., Int. Ed.* **2012**, *51*, 10413-10416.

(44) Lin, T. -E.; Lu, Y. -J.; Sun, C. -L.; Pick, H.; Chen, J. -P.; Lesch, A.; Girault, H. H. Soft Electrochemical Probes for Mapping the Distribution of Biomarkers and Injected Nanomaterials in Animal and Human Tissues. *Angew. Chem., Int. Ed.* **2017**, *56*, 16498-16502.

(45) Zhan, W.; Bard, A. J. Electrogenerated chemiluminescence. 83. Immunoassay of human C-reactive protein by using Ru(bpy)$_3^{2+}$-encapsulated liposomes as labels. *Anal. Chem.* **2007**, *79*, 459-463.

(46) Glasscott, M. W.; Voci, S.; Kauffmann, P. J.; Chapoval, A. I.; Dick, J. E. Mapping Solvent Entrapment in Multiphase Systems by Electrogenerated Chemiluminescence. *Langmuir* **2021**, *37*, 2907–2912.

(47) Glasscott, M.W.; Dick, J. E. Visualizing Phase Boundaries with Electrogenerated Chemiluminescence. *J. Phys. Chem. Lett.* **2020**, *11*, 4803–4808.

(48) Bard, A. J. *Electrogenerated Chemiluminescence*; M. Dekker, New York, **2004**.

(49) Hesari, M.; Ding, Z. Review-Electrogenerated Chemiluminescence: Light Years Ahead. *J. Electrochem. Soc.* **2016**, *163*, H3116-H3131.

(50) Liu, Z.; Qi, W.; Xu, G. Recent advances in electrochemiluminescence. *Chem. Soc. Rev.* **2015**, *44*, 3117-3142.

(51) Abdussalam, A.; Xu, G. Recent advances in electrochemiluminescence luminophores. *Anal. Bioanal. Chem.* **2021**, https://doi-org.inc.bib.cnrs.fr/10.1007/s00216-021-03329-0.

(52) Zhang, J.; Arbault, S.; Sojic, N.; Jiang, D. Electrochemiluminescence Imaging for Bioanalysis. *Annual Rev. Anal. Chem.* **2019**, *12*, 275-295.

(53) Dang, Q.; Gao, H.; Li, Z.; Qi, H.; Gao, Q.; Zhang, C. Simple and sensitive electrogenerated chemiluminescence peptide-based biosensor for detection of matrix metalloproteinase 2 released from living cells. *Anal. Bioanal. Chem.* **2016**, *408*, 7067-7075.

(54) Blackburn, G. F.; Shah, H. P.; Kenten, J. H.; Leland, J.; Kamin, R. A.; Link, J.; Peterman, J.; Powell, M. J.; Shah, A.; Talley, D. B.; Tyagi, S. K.; Wilkins, E.; Wu, T. -G.; Massey, R. J. Electrochemiluminescence Detection for Development of Immunoassays and DNA Probe Assays for Clinical Diagnostics. *Clin. Chem.* **1991**, *37*, 1534-1539.

(55) Sardesai, N.; Pan, S.; Rusling, J. Electrochemiluminescent immunosensor for detection of protein cancer biomarkers using carbon nanotube forests and [Ru-(bpy)(3)](2+)-doped silica nanoparticles. *Chem. Commun.* **2009**, 4968-4970.

(56) Wilson, A. J.; Marchuk, K.; Willets, K. A. Imaging Electrogenerated Chemiluminescence at Single Gold Nanowire Electrodes. *Nano Lett.* **2015**, *15*, 6110-6115.

(57) Sentic, M.; Milutinovic, M.; Kanoufi, F.; Manojlovic, D.; Arbault, S.; Sojic, N. Mapping electrogenerated chemiluminescence reactivity in space: mechanistic insight into model systems used in immunoassays. *Chem. Sci.* **2014**, *5*, 2568-2572.

(58) Deiss, F.; LaFratta, C. N.; Symer, M.; Blicharz, T. M.; Sojic, N.; Walt, D. R. Multiplexed Sandwich Immunoassays Using Electrochemiluminescence Imaging Resolved at the Single Bead Level. *J. Am. Chem. Soc.* **2009**, *131*, 6088-6089.

(59) Valenti, G.; Zangheri, M.; Sansaloni, S. E.; Mirasoli, M.; Penicaud, A.; Roda, A.; Paolucci, F. Transparent Carbon Nanotube Network for Efficient Electrochemiluminescence Devices. *Chem. Eur. J.* **2015**, *21*, 12640-12645.

(60) Dick, J. E.; Renault, C.; Kim, B. -K.; Bard, A. J. Simultaneous Detection of Single Attoliter Droplet Collisions by Electrochemical and Electrogenerated Chemiluminescent Responses. *Angew. Chem., Int. Ed.* **2014**, *53*, 11859-11862.

(61) Fan, F. -R. F.; Park, S.; Zhu, Y.; Ruoff, R. S.; Bard, A. J. Electrogenerated Chemiluminescence of Partially Oxidized Highly Oriented Pyrolytic Graphite Surfaces and of Graphene Oxide Nanoparticles. *J. Am. Chem. Soc.* **2009**, *131*, 937-939.

(62) Zhu, M. -J.; Pan, J. -B.; Wu, Z. -Q.; Gao, X. -Y.; Zhao, W.; Xia, X. -H.; Xu, J. -J.; Chen, H. -Y. Electrogenerated Chemiluminescence Imaging of Electrocatalysis at a Single Au-Pt Janus Nanoparticle. *Angew. Chem., Int. Ed.* **2018**, *57*, 4010-4014.

(63) Xu, J.; Huang, P.; Qin, Y.; Jiang, D.; Chen, H. -Y. Analysis of Intracellular Glucose at Single Cells Using Electrochemiluminescence Imaging. *Anal. Chem.* **2016**, *88*, 4609-4612.

(64) Zhou, J.; Ma, G.; Chen, Y.; Fang, D.; Jiang, D.; Chen, H. -Y. Electrochemiluminescence Imaging for Parallel Single-Cell Analysis of Active Membrane Cholesterol. *Anal. Chem.* **2015**, *87*, 8138-8143.

(65) Ma, G.; Zhou, J.; Tian, C.; Jiang, D.; Fang, D.; Chen, H. -Y. Luminol Electrochemiluminescence for the Analysis of Active Cholesterol at the Plasma Membrane in Single Mammalian Cells *Anal. Chem.* **2013**, *85*, 3912-3917.

(66) Liu, G.; Ma, C.; Jin, B. -K.; Chen, Z. X.; Zhu, J. -J. Direct Electrochemiluminescence Imaging of a Single Cell on a Chitosan Film Modified Electrode. *Anal. Chem.* **2018**, *90*, 4801-4806.

(67) Valenti, G.; Scarabino, S.; Goudeau, B.; Lesch, A.; Jovic, M.; Villani, E.; Sentic, M.; Rapino, S.; Arbault, S.; Paolucci, F.; Sojic, N. Single Cell Electrochemiluminescence Imaging: From the Proof-of-Concept to Disposable Device-Based Analysis. *J. Am. Chem. Soc.* **2017**, *139*, 16830-16837.

(68) Voci, S.; Goudeau, B.; Valenti, G.; Lesch, A.; Jovic, M.; Rapino, S.; Paolucci, F.; Arbault, S.; Sojic, N. Surface-Confined Electrochemiluminescence Microscopy of Cell Membranes. *J. Am. Chem. Soc.* **2018**, *140*, 14753-14760.

(69) Ma, Y.; Colin, C.; Descamps, J.; Arbault, S.; Sojic, N. Shadow Electrochemiluminescence Microscopy of Single Mitochondria. *Angew. Chem., Int. Ed.* **2021**, *60*, 18742-18749.

(70) Deiss, F.; LaFratta, C. N.; Symer, M.; Blicharz, T. M.; Sojic, N.; Walt, D. R. Multiplexed Sandwich Immunoassays Using Electrochemiluminescence Imaging Resolved at the Single Bead Level. *J. Am. Chem. Soc.* **2009**, *131*, 6088–6089.

(71) Miao, W. J.; Choi, J.; Bard, A. J. Electrogenerated chemiluminescence 69: The tris(2,2 '-bipyridine)ruthenium(II), (Ru(bpy)(3)(2+))/tri-n-propylamine (TPrA) system revisited - A new route involving TPrA(center dot+) cation radicals. *J. Am. Chem. Soc.* **2002***, 124*, 14478–14485.

(72) Sentic, M.; Milutinovic, M.; Kanoufi, F.; Manojlovic, D.; Arbault, S.; Sojic, N. Mapping electrogenerated chemiluminescence reactivity in space: mechanistic insight into model systems used in immunoassays. *Chem. Sci.* **2014***, 5*, 2568–2572.

(73) Menger, F. M.; Keiper, J. S. Chemistry and physics of plant vesicles as biomembrane models. *Curr. Opin. Chem. Biol.* **1998**, *2*, 726-732.

(74) Dobereiner, H. -G. Properties of giant vesicles. *Curr. Opin. Colloid Interface Sci.* **2000**, *5*, 256-263.

(75) Messina, P.; Lemaître, F.; Huet, F.; Ngo, K. A.; Vivier, V.; Labbé, E.; Buriez, O.; Amatore, C. Monitoring and Quantifying the Passive Transport of Molecules Through Patch-Clamp Suspended Real and Model Cell Membranes. *Angew. Chem., Int. Ed.* **2014**, *53*, 3192–3196.

(76) Perez Jimenez, A. I.; Challier, L.; Aït-Yahiatène, E.; Delacotte, J.; Labbé, E.; Buriez, O. Selective Electrochemical Bleaching of the Outer Leaflet of Fluorescently Labeled Giant Liposomes. *Chem. Eur. J.* **2017**, *23*, 6781 – 6787

(77) Xia, Y.; Whitesides, G. M. Soft lithography. *Annu. Rev. Mater. Sci.* **1998**, *28*, 153-184.

(78) Deng, N.N.; Yelleswarapu, M.; Huck, W.T.S. Monodisperse Uni- and Multicompartment Liposomes. *J. Am. Chem. Soc.* **2016**, *138*, 7584-7591

(79) Reviakine, I.; Brisson, A. Formation of supported phospholipid bilayers from unilamellar vesicles investigated by atomic force microscopy. *Langmuir* **2000**, *16*, 1806–1815.

(80) Hardy, G. J.; Nayak, R.; Zauscher, S. Model cell membranes: Techniques to form complex biomimetic supported lipid bilayers via vesicle fusion. *Curr. Opin. Colloid. Interface Sci.* **2013**, *18*, 448–458.

(81) Granqvist, C. G.; Hultaker, A. Transparent and conducting ITO films: new developments and applications. *Thin Solid Films* **2002**, *411*, 1-5.

(82) Hosono, H.; Ohta, H.; Orita, M.; Ueda, K. Hirano, M. Frontier of transparent conductive oxide thin films. *Vacuum* **2002**, *66*, 419-425.

(83) Amatore, C.; Arbault, S.; Guille, M.; Lemaître, F. Electrochemical monitoring of single cell secretion: Vesicular exocytosis and oxidative stress. *Chem. Rev.* **2008**, *108*, 2585-2621.

(84) Amatore, C.; Arbault, S.; Bouret, Y.; Guille, M.; Lemaître, F.; Verchier, Y. Regulation of Exocytosis in Chromaffin Cells by Trans-Insertion of Lysophosphatidylcholine and Arachidonic Acid into the Outer Leaflet of the Cell Membrane. *ChemBioChem.* **2006**, *7*, 1998-2003.

(85) Amatore, C.; Arbault, S.; Bouton, C.; Drapier, J.-C.; Ghandour, H.; Koh, A.C.W. Real-Time Amperometric Analysis of Reactive Oxygen and Nitrogen Species Released by Single Immunostimulated Macrophages. *ChemBioChem.* **2008**, *9*, 1472 – 1480.

Table of Content Graphic